Experimental study of hydraulic transport of large particles in horizontal and S-shape pipes

Florent Ravelet, Farid Bakir, Sofiane Khelladi, Robert Rey

Experimental study of hydraulic transport of large particles in horizontal and S-shape pipes

F. Ravelet[a,*], F. Bakir[a], S. Khelladi[a], R. Rey[a]

[a] *Arts et Metiers ParisTech, DynFluid, 151 boulevard de l'Hôpital, 75013 Paris, France.*

Abstract

We study the pressure drop and flow regimes for a two-phase liquid and solid mixture that flows in a horizontal pipe and in a vertical S-shaped pipe. Two densities are used for the solids. The solids are spheres that are large with respect to the diameter of the pipe (5, 10 and 15%) or real stones of arbitrary shapes but constant density and a size distribution similar to the tested spherical beads. Finally, we study mixtures of size and / or density. The regimes are charaterized with differential pressure measurements and visualizations. The results show that the grain size and density have a strong effect on the transition point between regimes with a stationary bed and dispersed flows. The pressure drops are moreover smaller for large particles in the horizontal part. In order to match the pressure drop measurements, empirical models based on a Froude number are tested, together with 1D models that are based on mass and momentum balance. Finally, compared to vertical geometries, the pressure drops in horizontal pipes are significantly lower, but the critical velocities with respect to plugging are higher.

Keywords: Hydraulic transport, solid-liquid two-phase flow, bed friction, deep sea mining.

1. Introduction

The hydraulic transport of solid particles is a method widely used in chemical and mining industries. Many predictive models exist in the case of suspensions, that is to say when the particle diameter is small compared to the diameter of the pipe [1–3]. It is then possible to predict the pressure losses in horizontal or vertical pipes. In recent years, the sharp increase in demand for raw materials makes it interesting exploitation of new resources, particularly the use of fields at the bottom of the ocean [4].

In this case, the solids may be large with respect to the pipe diameter and the circuit would have complex shapes, including vertical parts, horizontal parts, and potentially bends and S-shapes in order to absorb the deformations caused by surface waves. For transport in vertical pipe, there are predictive models based on the work of Newitt *et al.* [5] and Richardson *et al.* [6]. We checked the validity of one model on a set of experimental data [7–9]. However, in horizontal, and a fortiori in geometries in S-shape, there are few models [1–3, 10, 11] and the effects of density and particle size have not been systematically explored. One major difficulty in the case of transport of large particles and high density comes from the various flow regimes that may be observed [1, 2, 10–13]: when the speed of transportation increases, several transitions arise from regimes with a layer of solids at the bottom of the pipe that is at rest or that flows backwards in inclined pipes [11–13] to regimes with a moving bed and eventually to heterogeneous and pseudo-homogeneous suspensions at high mixture velocities.

The knowledge of the velocity above which the bed starts to move forward is of great interest with respect to operation of a production line. Below this limit the system may indeed plug. In the present study, experiments are carried out in order to better understand the effects of solid size and density on this velocity. The solid/liquid mixture flows in a horizontal circular pipe and in a vertical S-shape pipe. The experimental set-up is presented in § 2. The results are presented in § 3. Some general considerations on the typical regimes and pressure drop curves that are observed in the system are presented in § 3.1. The main results concern mono-disperse calibrated solid spheres with two different sizes and two densities, flowing in the horizontal pipe and are presented in § 3.2. Mixture of spheres and rough stones of arbitrary shapes are also tested in § 3.3, in order to check to what extent the results obtained for spheres may represent an actual application. Several models are proposed and compared to the experiments in § 4. Conclusions and perspectives are then given in § 5.

2. Experimental set-up

2.1. Test loop

The test loop is shown schematically in Fig. 1. It consists of a first rigid, transparent horizontal pipe of internal diameter $D = 100$ mm and 10 m long in which flows the

*corresponding author
Email address: florent.ravelet@ensta.org (F. Ravelet)

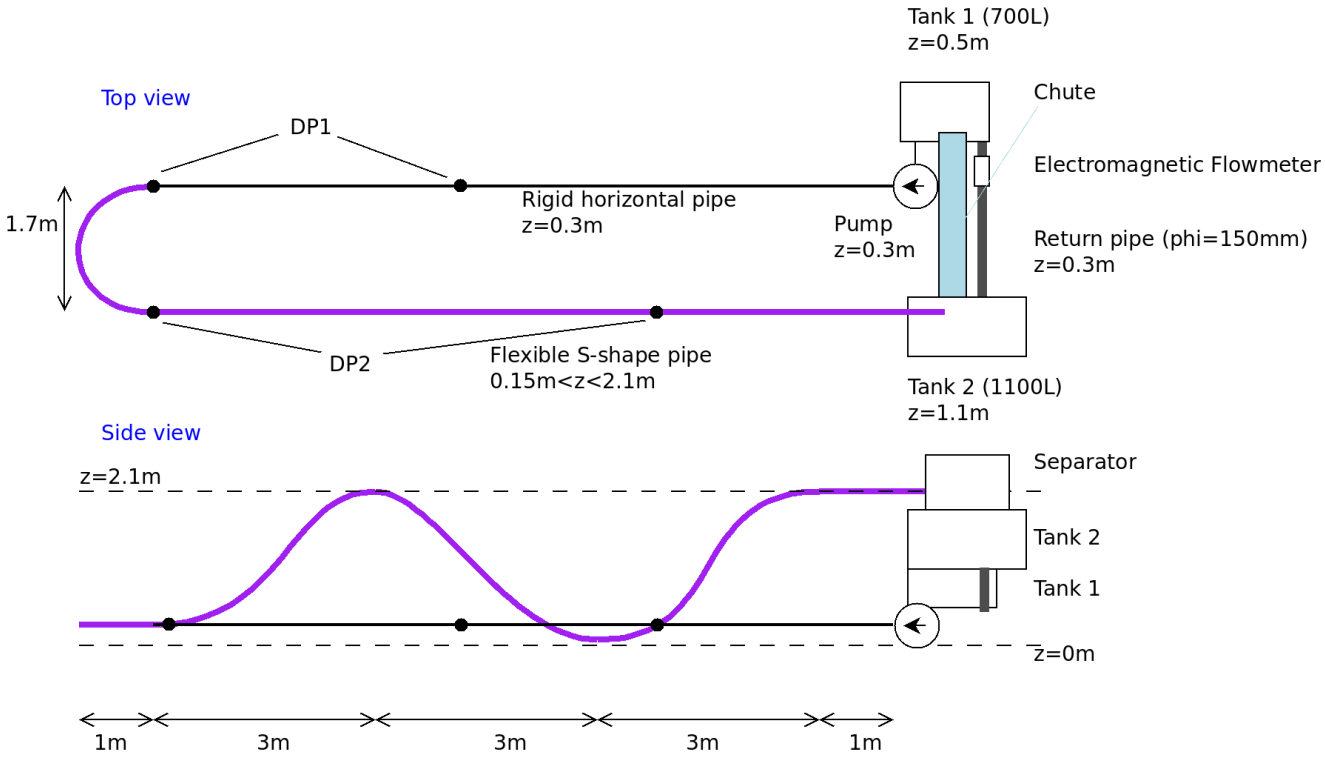

Figure 1: Sketch of the test loop. Top and side views.

liquid/solid mixture. The return occurs in a clear flexible PVC hose reinforced with a steel coil, of internal diameter $D = 100$ mm and total length 20 m. This return pipe first follows a 180^o horizontal curve of curvature diameter 1.7 m, then a climb, a descent and an ascent in a vertical plane.

The mixture of solids and water that flows in the rigid horizontal pipe and the return flexible pipe is then passed through a separator consisting of a closed box fitted with a side hatch and whose bottom side consists of a grid of stainless steel. The water then falls into the tank 2, and the solids flow in a chute that is inclined at 45^o. This chute provides at its end an adjustable flap in order to control the solids flow rate. The end of the chute is above a grid container of known capacity that is immerged in tank 1 and connected with a grid pipe to the outlet of tank 1. The separated water flows from tank 2 into tank 1 through a pipe with an electromagnetic flow-meter. The mixture is sucked by a vortex pump (Ensival Moret MT 100-100-250) connected to the outlet of tank 1 and delivered in the circuit.

2.2. Characteristics of the solids

Solids with different sizes and densities are used. Their physical and geometrical characteristics are summarized in Tab. 1. The particles are relatively large, with sizes ranging from 5% to 18% of the pipe diameter. We use calibrated beads of glass (SiLi, SiLibeads type M, with a relative dispersion of sizes of 4%) and of alumina (Umicore, Alumina Degussit 92%, with a relative dispersion of sizes of 10%). The real solids that are used from the perspective of an actual application have irregular shapes, as can be seen in the picture in Tab. 1. The density of a sample of fifty solids have been measured with a densimeter. It is constant within 2700 ± 10 kg.m^{-3}.

2.3. Control parameters and measured quantities

The aim of the present work is to measure the pressure drops in different parts of the test loop as a function of concentration and velocity. Several choices can be made for the definition of these quantities. The natural control parameters, *i.e.* the parameters that are really adjusted with experimental means, are the volumetric flow rates of the liquid (Q_l) and of the solids (Q_s).

We choose to use the following set of parameters for presenting the results. The first is the mixture velocity V_{mix} and the second is the *transport* or *delivered* concentration C:

$$V_{mix} = \frac{Q_l + Q_s}{A}$$

$$C = \frac{Q_s}{Q_s + Q_l}$$

with A the cross-section area of the pipe. The use of the mixture velocity is convenient for comparison to the models described in § 4.

Concerning the concentration, please note that on the one hand, the solids do not flow with the same velocity as water, because of their large size and of the large density

Type	Glass beads	Alumina beads	Mixture 1 (alumina)	Mixture 2 (alumina)	Mixture 3 (alumina/glass)	Stones
Size	5 mm 10 mm 16 mm	6 mm 15 mm	50% 6 mm 50% 15 mm D_{50}:10.5 mm	75% 6 mm 25% 15 mm D_{50}:8.25 mm	50% 6 mm alumina 50% 5 mm glass D_{50}:5.5 mm	$8-18$ mm D_{50}:10 mm
Density	2500 kg.m^{-3}	3650 kg.m^{-3}	3650 kg.m^{-3}	3650 kg.m^{-3}	3075 kg.m^{-3}	2700 kg.m^{-3}
Picture						

Table 1: Physical characteristics of the calibrated beads and of the different mixtures. The mean diameter D_{50} is such that 50% of the solids are greater than this size.

contrast —in other words there is a non-negligible *slip* velocity. On the other hand, in horizontal parts it is known that there are regimes with a stationary layer of solids at rest at the bottom of the pipe [10, 11]. There could thus be a great difference between the *transport* or *delivered* concentration C and the *in-situ*, *local* or *volumetric* concentration ϵ_s that is the ratio between the area occupied by the solids and the area of the pipe.

Our goal is to perform measurements with varying V_{mix} in the range 0—5 m.s^{-1}, for constant delivered concentrations of 5, 10, 15 et 20%.

The water flow-rate is measured using an electromagnetic flowmeter (KROHNE Optiflux 2000) and adjusted by varying the rotation rate of the vortex pump. The solids flow-rate is set through a hatch and is measured by filling the buffer zone of known capacity located in the tank 1. Finally, we measure the pressure drop using two differential pressure sensors (VEGADIF65): a first that is located at the end of the straight line, 60 diameters downward of the pump, and a second that is located at the hose in the S-shaped part (see the position of the pressure taps in Fig. 1). Data are recorded for 30 s at a sample rate of 130 Hz. Measuring the rate of fluctuation of flow and pressure is used as a validation criterion of the measurements. The losses are expressed in terms of hydraulic gradients (meters of water column per meter of pipe):

$$I(m/m) = \frac{\Delta P}{\rho_l g L}$$

with ΔP the measured static pressure drop, ρ_l the density of the carying liquid (water) and L the curvilinear distance between the pressure taps.

In the following, I_h stands for the hydraulic gradient in the horizontal line, and I_s stands for the hydraulic gradient in the S-shape pipe. The symbol I_v is used for the hydraulic gradient that would be observed in a vertical pipe.

Optical measurements are also performed with a high-speed camera (Optronis CamRecord600). Typically 3200 images are recorded with a resolution of 1280×1024 pixels at a frame rate of 200 Hz.

3. Results

3.1. Description of the different regimes

The Figure 2 presents a typical evolution of the hydraulic gradients I_h and I_s. The solids are glass beads of diameter 5 mm and the delivered concentration is $C = 5\%$.

The thick black line in Fig. 2 stands for the measured hydraulic gradient in the horizontal part in the case with water flowing alone. The typical Reynolds number is 2×10^5 and the flow is fully turbulent. The curve is a fit of the form $I = \lambda \frac{V^2}{2gD}$ that gives a value for the friction coefficients $\lambda_h = 0.156$ and $\lambda_s = 0.160$. Corresponding rugosities can be deduced with the Colebrook formula. The estimated rugosities are respectively 20 μm for the horizontal pipe, and 26 μm for the flexible PVC hose. The difference between the two hydraulic gradients in the two pipes is thus below 3%. Despite the presence of a few bends that may add singular pressure drops and of the reinforcement structure in the flexible pipe, the difference is low and only the curve concerning horizontal part is to be displayed in the following.

When dealing with a liquid/solid mixture (red •: I_h and blue ■: I_s in Fig. 2), the pressure drops are significantly higher for the whole range of mixture velocity. The green line is the results of a model for pressure drop in vertical flow, presented in § 4.1. Please note that the pressure drops in the horizontal and S-shape parts are lower than those expected for a vertical pipe. The red and blue lines

are fits of I_h and I_s that are drawn for visual comfort. The proposed functional dependence $I = a/V_{mix} + bV_{mix}^2$ will be justified in § 4.2.

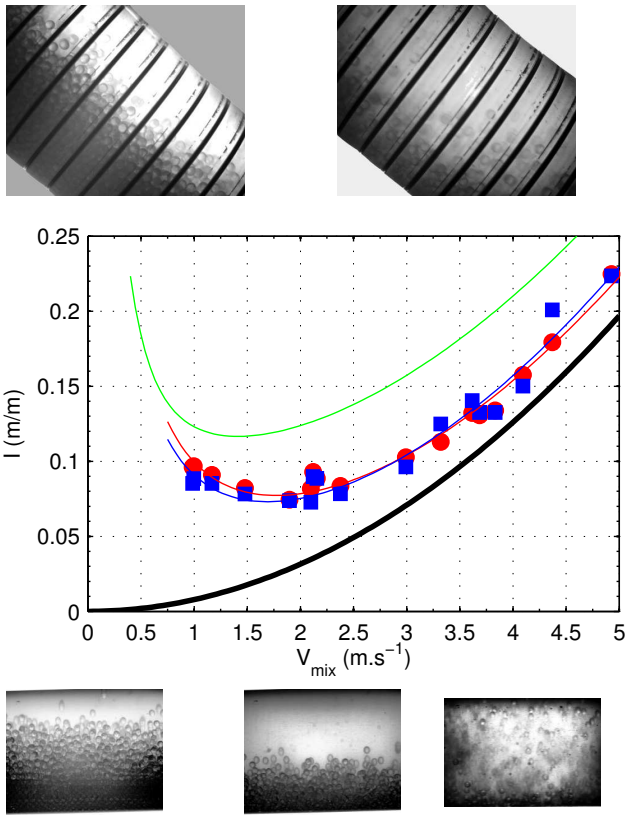

Figure 2: Illustration of the different regimes. Hydraulic gradient *vs.* V_{mix}, glass beads of 5 mm, $C = 5\%$. Solid black line: water flowing alone, red •: I_h, blue ■: I_s. The blue and red solid lines are fits of the type $a/V_{mix} + bV_{mix}^2$ (see § 4.2). The green solid line stands for the results of the model developed for vertical pipelines (see § 4.1).

A remarkable feature of the curves is the presence of a local minimum: the hydraulic gradient does not vary monotonically with the velocity. The mixture velocity for which the minimum hydraulic gradient is observed will be termed the *critical velocity* V_{crit}, following the definition of Doron *et al.* [10]. In the present case and in the horizontal pipe, the critical velocity is $V_{crit\,h} \simeq 1.8$ m.s^{-1}.

For $V_{mix} < V_{crit}$ in the horizontal pipes, flow regimes with a stationary bed above which a compact layer of beads is flowing are observed (see bottom left picture in Fig. 2 that corresponds to $V_{mix} = 1.2$ m.s^{-1}). The more the mixture velocity decreases, the more the solids tend to settle down. These regimes are thus such that $\epsilon_s >> C$ and are characterized by a large pressure drop that is caused by a decrease in the discharge section. In the ascending part of the flexible pipe, a layer of solids located at the bottom of the pipe and that is flowing backwards is even observed for these low velocities, as already observed by Yamaguchi *et al.* [13] (see top left picture in Fig. 2 that is taken at $V_{mix} = 0.9$ m.s^{-1}). The flow in this regime is very unstable and the transit time needed to reach a stationary state is very long, of the order of twenty minutes —the typical time for a solid to flow through the whole pipe being 30 s.

Slightly above the critical velocity —for $V_{mix} \gtrsim V_{crit}$— a bed on the bottom of the pipe that is sliding is observed both in the horizontal pipe and in the S-shaped part (see bottom central picture and top right picture in Fig. 2 that are both taken at $V_{mix} = 2.1$ m.s^{-1}). The velocity of this bed is small compared to the mixture velocity and $\epsilon_s > C$.

Increasing further the mixture velocity, more and more solid beads get suspended and transported by the flow. The pressure drop curves behave as the clear-water pressure drop curve and follow the same trend at high velocities. In that case, $\epsilon_s \gtrsim C$ and the regime is called "pseudo-homogeneous" (see bottom right picture in Fig. 2 that is taken at $V_{mix} = 4.9$ m.s^{-1}).

3.2. Effects of the physical characteristics of the beads

This paragraph is devoted to the comparison of the pressure drop curves with various concentrations, densities and sizes for identical spherical beads. The reference case is the Alumina beads of diameter 6 mm, density $\rho_s = 3650$ kg.m^{-3}, and at a delivered concentration $C = 5\%$. In this case, the order of magnitude of the minimal pressure drop at critical velocity $V_{crit\,h} \simeq 2.4$ m.s^{-1} is $I_{crit\,h} \simeq 0.11$ m/m.

The effects of the concentration are presented in Fig. 3a. Only results for the horizontal part are plotted. On the one hand, increasing the delivered concentration leads to an increase of the pressure drop, as expected. The pressure drop at critical point is increased by roughly 40% for $C = 10\%$ and for $C = 15\%$ the relative increase is roughly 70%. Very few points are available for the concentration $C = 20\%$ owing to the large power required; these points are nevertheless on both sides of the critical point. The increase in pressure drop at critical point is around 100%. On the other hand, changing the concentration seems to increase only very slightly the critical velocity (see § 4.2 for a discussion of this point). The effects are identical and of same order of magnitude for the S-shape pipe.

The comparison of two sizes of beads of same density at the same concentration is presented in Fig. 3b. The effects of the size are different for the horizontal pipe and the S-shape part. The pressure drop is indeed decreased for the bigger size in the horizontal pipe (open symbols in Fig. 3b), whereas the size has barely no effects in the S-shape part (closed symbols in Fig. 3b). The critical velocity moreover does not seem to be affected by the particle size. The decrease of pressure drop with larger particles and the constancy of the critical velocity are a distinguishing feature between horizontal and vertical flows as will be demonstrated in § 4.1.

Finally, increasing the density leads to both an increase of pressure drop and critical velocity, as illustrated in Fig. 3c in the horizontal part. One can also notice that though the pressure drops in the horizontal pipe and in

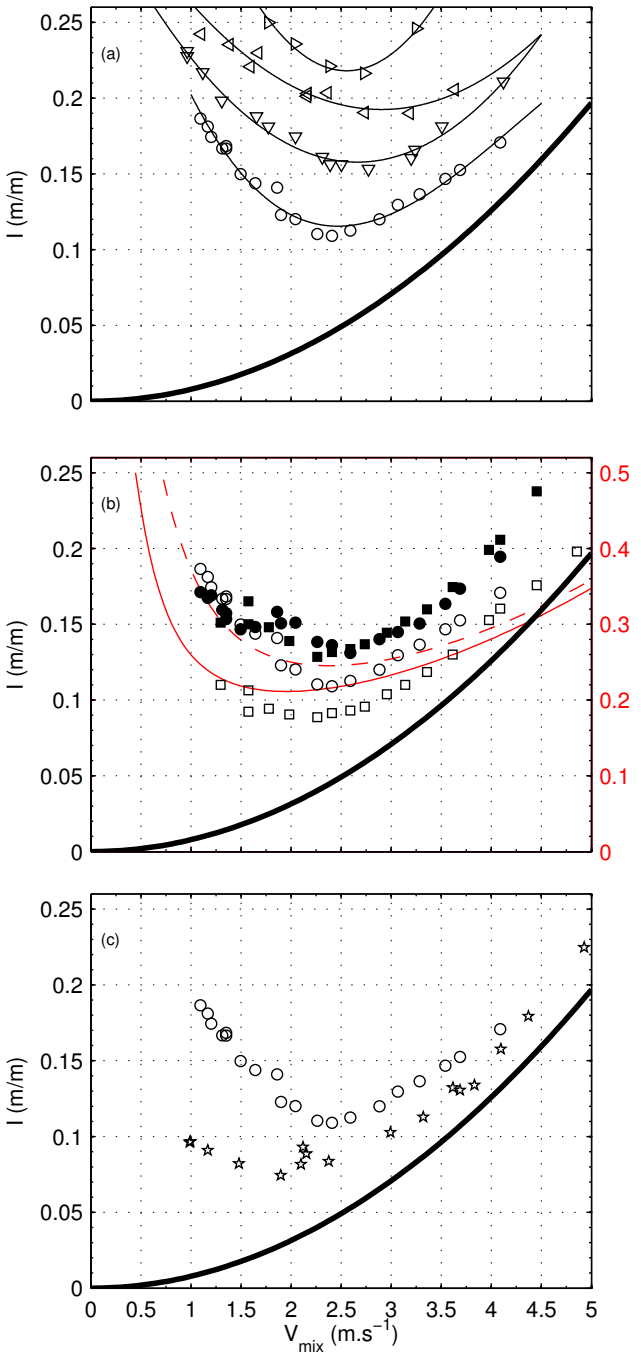

Figure 3: (a) I_h for 6 mm Alumina beads *vs.* V_{mix} at various concentrations. ○: $C = 5\%$, ▽: $C = 10\%$, ◁: $C = 15\%$ and ▷: $C = 20\%$. (b) I_h (open symbols) and I_s (filled symbols) for Alumina beads and $C = 5\%$ *vs.* V_{mix} for two sizes. ○: 6 mm and □: 15 mm. I_v computed with the model presented in § 4.1 for Alumina beads at $C = 5\%$ of diameter 6 mm (solid red line) and 15 mm (dashed red line). The ordinate axis is on the right (please note the factor 2 with respect to the left axis). (c) I_h for 5/6 mm and $C = 5\%$ *vs.* V_{mix} for two densities. ○: Alumina and ★: Glass.

the S-shape part are similar for the low density ($I_h \simeq I_s$ for glass beads of diameter 5 mm, see Fig. 2), the pressure drops in the two parts of the loop are different for the higher density ($I_s > I_h$ for alumina beads of diameter 5 mm, see Fig. 3b).

3.3. Mixes of beads and rough solids

This paragraph deals with mixtures of spheres and rough stones of arbitrary shapes in order to check to what extent the results obtained for mono-disperse spheres may represent an actual application.

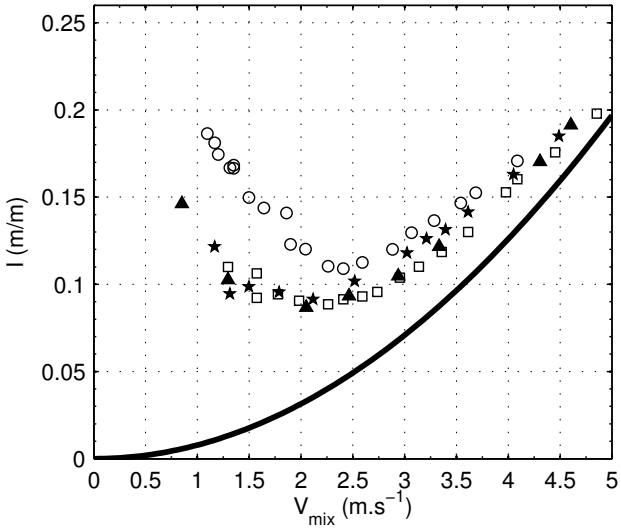

Figure 4: I_h at $C = 5\%$ *vs.* V_{mix}. ○: Alumina 6 mm, □: Alumina 15 mm, △: mixture 1 and ★: mixture 2.

The figure 4 presents the horizontal hydraulic gradient I_h *vs.* V_{mix} for different mixtures of alumina beads of diameter 6 mm and 15 mm. Contrary to what one might think *a priori*, the pressure drop of the mixtures is not a simple linear combination of the pressure drop of each bead size: for a 50% of 6 mm mixture (mixture 1) the pressure drop curve coincides with that of the 15 mm beads. The pressure drop is thus low. This effect is even still present for a proportion of 75% of 6 mm beads in the mixture (mixture 2) but only at low mixture velocities corresponding to $V_{mix} \lesssim V_{crit}$, *i.e.* to regimes with a stationary bed. For higher velocities the pressure drop lies between the other two and is closer to the pressure drop of the 6 mm beads.

The figure 5 presents the comparison of $I_h\,(V_{mix})$ for three mixtures of beads of same size but different density: glass beads of 5 mm (★), alumina beads of 6 mm (○) and mixture 3 (50% glass / 50% alumina, ◁). The pressure drop curve for the mixture lies between the two single-type cases and seems to be well modelized by the mean of the two curves: the solid red line in Fig. 5 is a fit for the alumina, the solid blue line a fit for glass and the black line is the mean of these two curves.

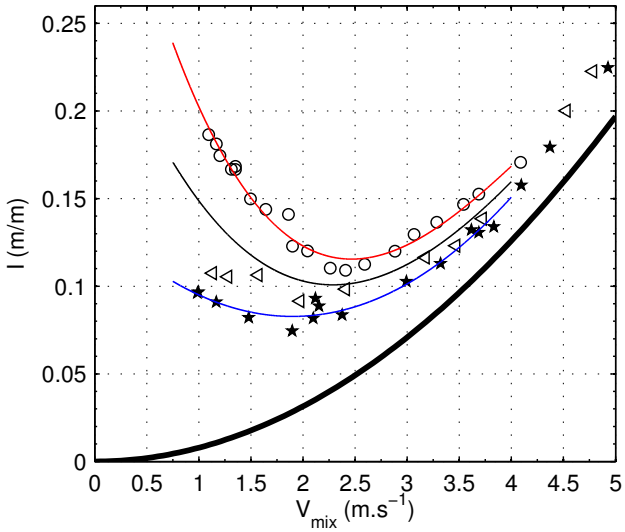

Figure 5: I_h at $C = 5\%$ *vs.* V_{mix}. ○: Alumina 6 mm with a fit corresponding to the red line, ★: Glass 5 mm with a fit corresponding to the blue line and ◁: mixture 3. The black solid line is the mean of the two fits.

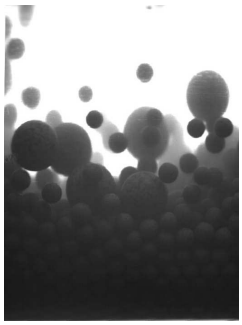

Figure 6: Illustration of segregation for mixture 2. In that case, $C = 5\%$ and $V_{mix} \simeq 1\text{m.s}^{-1}$.

The effects that have been observed for mixtures, particularly in the horizontal part, may be ascribed to segregation phenomena. This is illustrated in Fig. 6 for mixture 2 of alumina of two sizes (see Tab. 1). A tendency of having two layers of beads, with the small beads being transported at the bottom of the pipe while the large beads are transported on top of this bed, is indeed observed. This phenomenon is reminiscent of the so-called "Brazil nut effect". Likewise, for the mixture of beads of different densities, the heaviest tend to settle at the bottom of the pipe.

All the previous results concern experiments with spherical beads of unique size and density or mixtures of at most two different types of spherical beads. The pressure drop curves for stones are plotted in Fig. 7. Their physical characteristics are given and illustrated in Tab. 1. The density of a sample of fifty solids have been measured with a densimeter. It is constant within 2700 ± 10 kg.m^{-3}. Their density is thus very close to that of glass. Their size distribution is between 8 and 18 mm, with 50% of the solids

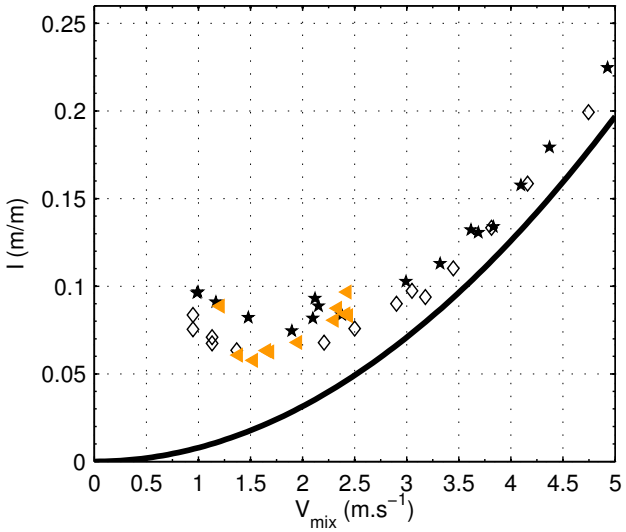

Figure 7: I_h at $C = 5\%$ *vs.* V_{mix}. ★: Glass 5 mm, ◇: Glass 10 mm and orange ◁: stones.

having a size lower than 10 mm. The pressure drop I_h for these solids is very close to the case of 10 mm glass beads. The irregular shape of the solids that leads to different drag coefficients thus does not seem to play an important role with respect to the hydraulic gradient, as already reported by Yoon *et al.* [9]. It may be a second order effect with respect to the size and density effects.

4. Modelisation

This section is devoted to the application of various models to the present data. The case of the S-shape part is not treated here and will be discussed in a forthcoming paper with new experimental data including a better discretisation of the different inclined parts and bends. The present section will thus focus on horizontal pipes, the case of solid-liquid flow in vertical pipes being of interest as a reference.

Different approaches are possible, including analytical predictive models based on physical considerations, empirical correlations, or computational fluid dynamics. In the present section, we first present an analytical model for vertical flow, we validate the model on different available data and give the predictions applied to our experimental parameters in § 4.1. We then try and compare our experimental data in the horizontal pipe to empirical correlations in § 4.2. Then we present results obtained with an analytical model based on mass and momentum balance for horizontal flows in § 4.3. Different prospects for numerical simulations are discussed in the conclusion (§ 5).

4.1. Model for vertical pipelines

The case of vertical flow is reasonably straightforward. The pressure force exerted on a column of fluid of height

z balances two forces: the hydrostatic weight of the mixture and the friction on pipe wall due to the fluid shear stress [1, 2]. In the following, the hydrostatic weight of the column of water is removed in order to present the hydraulic gradients that are due to the flow of a mixture in the pipe.

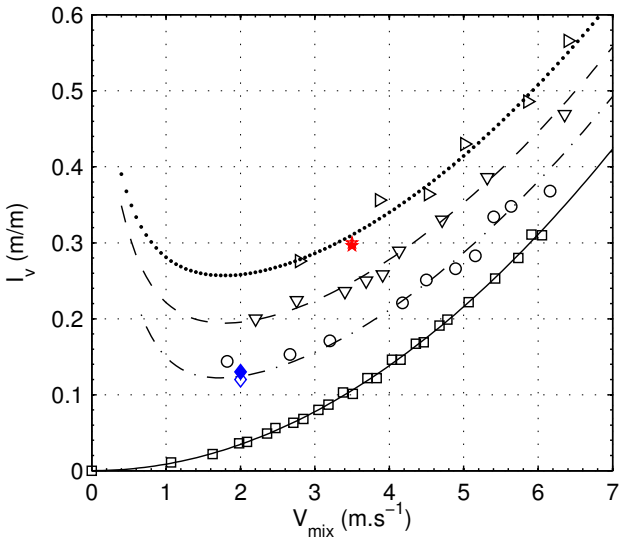

Figure 8: Validation of the vertical model on different data sets. Vertical hydraulic gradient I_v *vs.* mixture velocity V_{mix}. Black symbols: data of Yoon *et al.* [9] for spherical beads of diameter $d_p = 20$ mm, density $\rho_s = 2150$ kg.m^{-3} flowing in a pipe of diameter $D = 100$ mm, compared to the results of the model (black lines) for various concentrations (□ and filled line: $C = 0\%$, ○ and dash-dotted line: $C = 5\%$, ▽ and dashed line: $C = 10\%$ and ▷ and dotted line: $C = 15\%$). Red ★: data (open symbol) of Xia *et al.* [7] for spherical beads of diameter $d_p = 15$ mm, density $\rho_s = 2000$ kg.m^{-3} flowing in a pipe of diameter $D = 100$ mm, at $C = 15\%$, compared to the result of the model (closed symbol). Blue ♢: data (open symbol) of Hong *et al.* [8] for spherical beads of diameter $d_p = 5$ mm, density $\rho_s = 2500$ kg.m^{-3} flowing in a pipe of diameter $D = 50$ mm, at $C = 3.85\%$, compared to the result of the model (closed symbol).

The vertical hydraulic gradient I_v can thus be decomposed into two parts: $I_v = I_{stat} + I_f$, with I_{stat} the hydrostatic contribution and I_f the wall shear-stress contribution. The hydrostatic contribution reads:

$$I_{stat} = \frac{\rho_s - \rho_w}{\rho_w}\epsilon_s$$

The *in-situ* concentration ϵ_s is *a priori* unknown. Following the seminal work of Newitt *et al.* [5], the average velocity difference between the solids and the surrounding water, or *slip* velocity V_{slip} reads:

$$V_{slip} = \frac{1-C}{1-\epsilon_s}V_{mix} - \frac{C}{\epsilon_s}V_{mix} \qquad (1)$$

This slip velocity would be the terminal velocity V_0 for a single solid of diameter d_p and of drag coefficient $c_d = 0.44$ falling in an infinite medium of fluid at rest:

$$V_0 = \sqrt{\frac{4d_p g(\rho_s - \rho_w)}{3c_d\rho_w}}$$

However, it must be corrected in the case of a concentrated mixture flowing in a pipe. Owing to the range of parameters that we are interested in, we have chosen to use the Richardson & Zaki correlation [6] for the *hindered* average slip velocity:

$$V_{slip} = (1-\epsilon_s)^{2.4}V_0 \qquad (2)$$

The *in-situ* concentration is obtained by solving the non-linear system of Eqs. 1 and 2.

The model for the wall shear-stress contribution I_f is based on some asumptions. As noticed by Engelmann [14] or Hong *et al.* [8], large particles tend to migrate away from the wall due to hydrdynamic lift [2]. Assuming that the near-wall velocity profile is only slightly affected by the presence of particles in the core region, the wall shear-stress is modeled by water flowing at the water velocity:

$$I_f = \lambda\frac{(V_{mix}\frac{1-C}{1-\epsilon_s})^2}{2gD}$$

This model for vertical flow has been implemented in Matlab and has been validated on various experimental data available in the Literature [7–9]. The comparison between the model and the data is plotted in Fig. 8. The agreement is very good. The model is thus used with the parameters of the present experiments to compare the order of magnitude of hydraulic gradients and critical velocities between horizontal and vertical flows (see for instance Figs. 2 and 3b).

The main conclusions are first that the hydraulic gradient in the horizontal part is lower than the one that would be observed in a vertical pipe whatever the density or solid size. The main contribution in the vertical model comes from the hydrostatic pressure of the mixture that is thus greater than the contribution of the bed formation in horizontal configuration. And secondly, owing to the dependence of the slip velocity on the square root of the particle diameter, the hydraulic gradient and the critical velocity are greater for larger solids in verical flows, contrary to what is observed in horizontal flows.

4.2. Semi-empirical correlations based on Froude number

In this paragraph some correlations are tested on the experimental data. The first quantity that could be checked is the critical velocity V_{crit} that is the mixture velocity for which the minimum hydraulic gradient is observed. One correlation for this velocity is the one originally proposed by Durand & Condolios (1952) [1]:

$$V_{crit} = F_l\{2D\,g\,(\rho_s - \rho_w)/\rho_w\}^{1/2} \qquad (3)$$

with F_l a constant of order unity. This corresponds to the critical value 1 for a Froude number Fr based on the mixture velocity, the pipe diameter and taking into account the dimensionless density difference:

$$Fr = \frac{V_{mix}}{\sqrt{2gD\frac{\rho_s-\rho_w}{\rho_w}}}$$

	Glass 5 mm, $C = 5\%$	Alumina 6 mm, $C = 5\%$
Experiment	1.8	2.4
Eq. 3 with $F_l = 1$	1.7	2.3
Eq. 3 with $F_l = 1.05$	1.8	2.4

Table 2: Critical velocity V_{crit} (m.s^{-1}) experimentally measured for alumina and glass beads, compared to the values predicted with the correlation 3.

Among the numerous empirical correlations proposed in the literature for the hydraulic gradient I_h, one that is most likely to apply to our case is the correlation based on the works of Durand (1953) and that is discussed in Refs. [1, 10]. It is restricted to flow regimes in the vicinity of the critical velocity, with mixture velociies slightly below to three or four times greater. Two dimensionless numbers are introduced. The first dimensionless number is the previously introduced Froude number. The second dimensionless number represents the excess of head loss due to the transport of solids:

$$\Phi_t = \frac{I_h - I_w}{I_w}$$

with I_w the head loss of water alone that would flow at the velocity V_{mix}.

The original correlation reads:

$$\Phi_t = C\,K\,c_d^{-3/4}\,(\sqrt{2}Fr)^{-3} \qquad (4)$$

with the constant $K = 81$ as a recommended value [10]. The functional form of I_h that is predicted by this model is thus: $I_h = I_w\,(1 + AV_{mix}^{-3}) = bV_{mix}^2 + aV_{mix}^{-1}$, as displayed in Figs. 2 and 5.

One could furthermore notice that the particle diameter does not explicitly appear in the correlations 3 and 4. A strong (resp. slight) dependency of the hydraulic gradient (resp. the critical velocity) is however observed for particles of different size (see Fig. 3b): the constants of the models can not therefore be universal.

The results concerning the prediction of the critical velocity are reported in Tab. 2. The predicted values are in excellent agreement with the experimental values. The definition of the Froude number thus seems appropriate since the critical velocity corresponds to a Froude number of order unity for Glass and Alumina beads of various sizes and at various concentrations (see Figs. 3 for Alumina and 7 for Glass).

The value of the dimensionless excess of head loss Φ_t, normalized by the delivered concentration C is plotted as a function of the Froude number Fr for various data sets in Fig. 9. All the data follow the same trend, with a -3 power law. The effect of the concentration is well described by the linear dependence: the data points for Glass beads of 5 mm at a concentration $C = 5\%$ (★) and at a concentration $C = 10\%$ (◇) collapse on a single curve corresponding to a constant $K = 67 \pm 0.5$. The effect of density seems to be well taken into account in the definition of the Froude number: the data points for Glass beads of 5 mm at a concentration $C = 5\%$ (★) and for Alumina beads of 6 mm at a concentration $C = 5\%$ (○) are very close, the values of the constant K being respectively 67 and 64. As already noticed, the size of the particles, that is not taken into account in the model, has a strong influence on the hydraulic gradient: The value of the constant for Glass beads of 10 mm (not represented in Fig. 9) is indeed $K = 47$ and the value for Alumina beads of 15 mm (□) is $K = 40$.

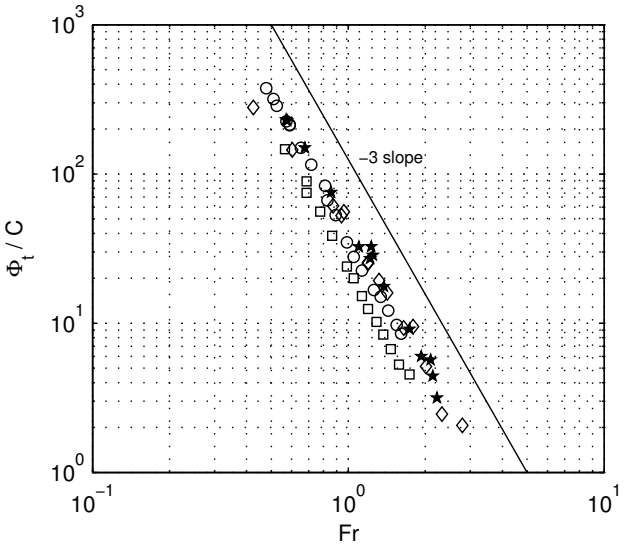

Figure 9: Dimensionless excess of head loss divided by the delivered concentration Φ_t/C *vs.* Froude number Fr for ★: Glass beads of 5 mm ($C = 5\%$), ◇: Glass beads of 5 mm ($C = 10\%$), ○: Alumina beads of 6 mm ($C = 5\%$) and □: Alumina beads of 15 mm ($C = 5\%$).

4.3. Analytical model based on mass and momentum balance

Doron *et al.* [10] have established an analytical model for slurry flow in horizontal pipes. This model is based on the decomposition of the cross-section of the pipe into two layers. It is thus a one dimensional model. The bottom of the pipe is assumed to be filled with a stationary or moving bed of packed particles. The height of this bed is y_b and the volumetric concentration in this layer is $C_b = 0.52$. An heterogeneous mixture of solids and fluid is flowing in the upper part of the pipe. The mixture is treated as an homogeneous fluid with averaged physical properties and no

slip between the phases is considered. The mass and momentum balance are then written in each layer. The shear stresses at the walls and at the interface between the two layers are modeled with frictions coefficients, and with a static friction force for the lower layer. In addition, the dispersion process of the solid particles in the upper layer is modeled by a turbulent diffusion process balanced by the gravitational settling of particles, leading to an advection-diffusion equation. The size of the particles is taken into account, firstly to define the roughness of the interface between the two layers, and secondly in the definition of the turbulent diffusion coefficient and the advection velocity that is the hindered terminal velocity.

This model leads to a non-linear system of 5 equations with 5 unknowns: the bed height (y_b), the velocity of the upper layer (U_h), the velocity of the lower layer (U_b), the concentration in the upper layer (C_h) and the pressure gradient (∇P). We have implemented this model in Matlab, and the non-linear system is solved in an iterative way, with a trust-region dogleg algorithm.

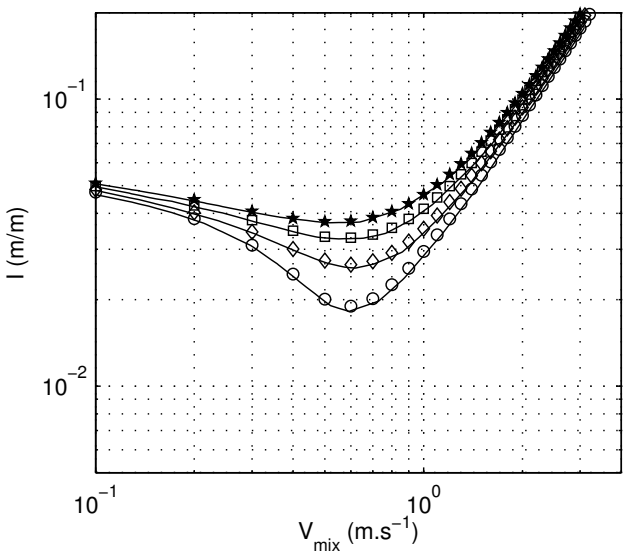

Figure 10: Validation of the two-layer model on data extracted from Fig. 3 of Ref. [10] for particles of diameter $d_p = 3$ mm, density $\rho_s = 1240$ kg.m^{-3} flowing in an horizontal pipe of diameter $D = 50$ mm for various concentrations. Symbols: results of our model, with $\eta = 0.3$, $\tan\phi = 0.6$ and $C_b = 0.52$, for ∘: $C = 4.2\%$, ◇: $C = 7.6\%$, □: $C = 11.2\%$ and ★: $C = 15.5\%$. Solid lines: curves extracted from Ref. [10].

The parameters of the model are: the solid friction coefficient between the pipe wall and the particles (η), an angle of internal friction that models the normal stress transmitted by the shear stress at the interface between the fluid and the bed (Φ), the packing concentration (C_b) and the correlations for fluid friction coefficients. In the original work of Doron *et al.* [10], the values of the parameters are the following: $\eta = 0.3$, $\tan\Phi = 0.6$ and $C_b = 0.52$. The physical properties of the solids are a low density of 1240 kg.m^{-3} and a particle to pipe diameter ratio of 6%. The figure 10 presents the results of our implementation of the model compared to the original work. Our implementation is thus validated.

The question we adress is to what extent it may apply to the present physical parameters, with solids of much higher density and even higher relative diameter.

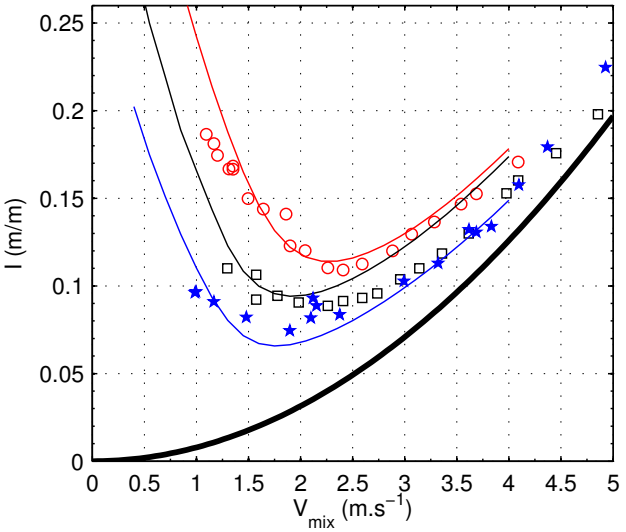

Figure 11: Results of the model (solid lines) compared to the present experimental data (symbols) at $C = 5\%$. Blue line and ★: Glass 5 mm. Red line and ∘: Alumina 6 mm. Black line and □: Alumina 15 mm. Parameters for the model: $C_b = 0.52$, $\eta = 0.25$, $\tan\Phi = \infty$ (see text).

We have first experimentally measured the packing concentration C_b by weighting a tube of same diameter and capacity two liters filled with dry beads and with beads and water. A dozen of measurements have been performed for each type of bead. The concentration is found to be 0.52 ± 0.01. The determination of the solid friction coefficient for an immersed granular bed is a very difficult problem [15], and the friction coefficient itself can strongly vary with the beads roughness [16]. We thus choose to vary η and to present the results that better match the experimental data in the vicinity of the critical velocity. The angle Φ is set to $\Phi = \pi/2$ which corresponds to neglecting the contribution of the normal stress transmitted into the bottom layer by the shear at the interface. This asumption is validated *a posteriori* by evaluation of its relative contribution.

The results for the hydraulic gradient are presented in Fig. 11. The final value of the friction coefficient is $\eta = 0.25$. The predictions of the model for the two small beads of different density and relative diameter 5% are in relatively good accordance with the experiments. For the largest beads, the trend of the reduction of the hydraulic gradient is reproduced but the model is not satisfactory: it matches the data point only very close to the critical velocity.

The models also predicts the height of the lower layer and the velocities of the two layers. Some pictures taken for the glass beads at $C = 5\%$ are presented in Fig. 12

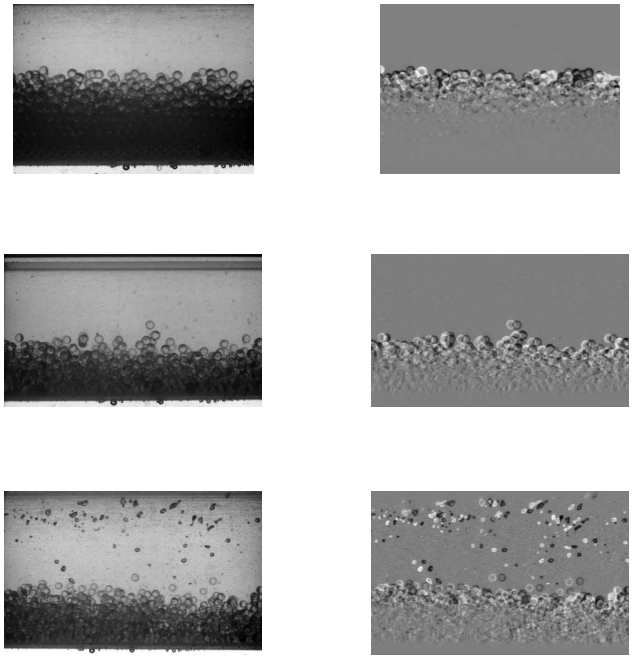

Figure 12: Pictures taken in the horizontal pipe of Glass beads of diameter 5 mm at $C = 5\%$. Left column: rough picture. Right column: difference between two successive images taken at the frame rate f. From top to bottom: $V = 1.0$ m.s^{-1} & $f = 50$ Hz, $V = 1.9$ m.s^{-1} & $f = 500$ Hz and $V = 3.9$ m.s^{-1} & $f = 630$ Hz.

at different velocities. The right column corresponds to the difference between two successive images and allows to better identify the different flow regimes and layers. At $V = 1.0$ m.s^{-1}, the bottom layer is static. The height of this static bed is roughly 42 mm while the value predicted by the model is 40 mm. At $V = 1.9$ m.s^{-1}, the bottom layer is moving slowly. The height of the moving bed is roughly 25 mm while the value predicted by the model is 22 mm. And finally, at $V = 3.9$ m.s^{-1}, one can still distinguish two layers of solids, with a bottom layer that is moving more rapidly. The height of this static bed is roughly 22 mm while the value predicted by the model is 15 mm. The velocities that are evaluated with the movies give similar accordance.

In conclusion, this two-layer model, originally validated only on small density particles, is promising and predicts well the global and few local features of the two-phase flow for larger densities. It seems however limited to not too large particles.

5. Discussion and Conclusion

We have thus measured the hydraulic gradient as a function of mixture velocity for calibrated beads of two densities (2500 kg.m^{-3} and 3650 kg.m^{-3}), with large particle to pipe diameter ratios of 5, 10 and up to 15%, as well as mixtures of calibrated beads and real stones of similar physical properties. The tests have been conducted mainly in in an horizontal pipe and also in a vertical S-shaped pipe. The main results are the following:

- The hydraulic gradient for horizontal and for the total S-shape pipe are lower than those who would be observed in a vertical pipe. On the other hand, the critical velocities that are a key parameter with respect to plugging for the design of a complex industrial application are greater.
- For a given density and delivered concentration, the hydraulic gradient decreases with the increase of the particle size in an horizontal pipe, contrary to what is observed in vertical pipes.
- The empirical correlations that are available in the Literature give satisfactory results but the classical constants that are recommended clearly do not correspond to the present case of very large particles. Further studies with even larger beads are necessary to better model the variation of these constants with the particle size.
- The mixtures and real stones could be modeled with mono-dispersed beads of equivalent densities and size. However, at low velocities, strong segregation mechanisms are present and would make the modelisation harder.
- Analytical models based on more physical arguments are of great interest. They however show their limits for the largest beads.

This last point may be linked to the fact that for large beads, the modelisation of the solids by a continuum medium, even with the help of granular theory becomes very untrustworthy. The number of particles that can be put in the pipe cross-section is too small to be treatred with statistical methods. For instance, numerical methods with Eulerian-Eulerian formulation such as the one presented in Ref. [17] is unappropriate to our case and even give unpresentable results. Lagrangian methods would also be very expensive owing to the nevertheless large number of particles. We are now developping alternate methods based on volume penalization [18] that seem very promising.

Further experiments are scheduled in the S-shape part, and in inclined pipes.

Acknowledgement

We would like to thank the Technip company for financial support, especially J. Denegre, P. Espinasse and T. Parenteau. We are particularly indebted to M. Joulin from the DynFluid laboratory of Arts et Metiers ParisTech, as well as to the students J.-R. De Céa and C. Valet for their assistance in the design and development of the experiment. The main part of the experiments have been carried out with the help of A. Lemaire.

[1] P.E. Baha Abulnaga. *Slurry Systems Handbook*. McGraw-Hill, 2002.

[2] K. C. Wilson, G. R. Addie, A. Sellgren, and R. Clift. *Slurry Transport Using Centrifugal Pumps*. Springer, 2006.

[3] V. Matousek. Predictive model for frictional pressure drop in settling-slurry pipe with stationary deposit. *Powder Technology*, 192:367–374, 2009.

[4] K. Pougatch and M. Salcudean. Numerical modeling of deep sea air-lift. *Ocean Engineering*, 35:1173, 2008.

[5] D. M. Newitt, J. F. Richardson, and B. J. Gliddon. Hydraulic conveying of solids in vertical pipes. *Trans. Instn. Chem. Engrs.*, 39:93–100, 1961.

[6] J. F. Richardson and W. N. Zaki. Sedimentation and fluidisation. *Trans. Inst. Chem. Engrs.*, 32:35–53, 1957.

[7] J. X. Xia, J. R. Ni, and C. Mendoza. Hydraulic lifting of manganese nodules through a riser. *J. Offshore Mechanics and Arctic Engineering*, 126:72, 2004.

[8] S. Hong, J. Choi, and C. K. Yang. Experimental study on solid-water slurry flow in vertical pipe by using ptv method. In *Proceedings of the Twelfth (2002) International Offshore and Polar Engineering Conference*, pages 462–466, 2002.

[9] C. H. Yoon, J. S. Kang, Y. C. Park, Y. J. Kim, J. M. Park, and S. K. Kwon. Solid-liquid flow experiment with real and artificial manganese nodules in flexible hoses. In *Proceedings of the Eighteenth (2008) International Offshore and Polar Engineering Conference*, pages 68–72, 2008.

[10] P. Doron, D. Granica, and D. Barnea. Slurry flow in horizontal pipes - experimental and modeling. *Int. J. Multiphase Flow*, 13:535–547, 1987.

[11] P. Doron, M. Simkhis, and D. Barnea. Flow of solid-liquid mixtures in inclined pipes. *Int. J. Multiphase Flow*, 23:313–323, 1997.

[12] V. Matousek. Pressure drops and flow patterns in sand-mixture pipes. *Experimental thermal and fluid science*, 26:693–702, 2002.

[13] H. Yamaguchi, X.-D. Niu, S. Nagaoka, and F. de Vuyst. Solid-liquid two-phase flow measurement using an electromagnetically induced signal measurement method. *J. Fluids Eng.*, 133:041302, 2011.

[14] H. E. Engelmann. Vertical hydraulic lifting of large-size particles — a contribution to marine mining. In *10^{th} Off. Tech. Conf.*, pages 731–740, 1978.

[15] T. Divoux and J.-C. Géminard. Friction and dilatancy in immersed granular matter. *Physical review letters*, 99:258301, 2007.

[16] N. A. Pohlman, B. L. Severson, J. M. Ottino, and R. M. Lueptow. Surface roughness effects in granular matter: Influence on angle of repose and the absence of segregation. *Physical Review E*, 73:031304, 2006.

[17] J. Ling, P. V. Skudarnov, C. X. Lin, and M. A. Ebadian. Numerical investigations of liquid-solid slurry flows in a fully developed turbulent flow region. *Int. J. Heat and Fluid Flow*, 24:389–398, 2003.

[18] D. Kolomenskiy and K. Schneider. A fourier spectral method for the navier-stokes equations with volume penalization for moving solid obstacles. *Journal of Computational Physics*, 228:5687–5709, 2009.